Unexpected Early Proteomic Changes in Alzheimer's Disease Model Mice Synaptosomes

Kerri Ball[1], Addolorata Pisconti[1], Kelly Grounds[1], William M. Old[1,*], Michael H. B. Stowell[1,2,*]

[1]The Department of Molecular, Cellular, and Developmental Biology, University of Colorado, Boulder, Colorado 80309-0347

[2]The Department of Mechanical Engineering, University of Colorado, Boulder, Colorado 80309-0347

This work supported in part by the NIH (M.H.B.S.) and HHMI (M.H.B.S.)

*To whom correspondence should be addressed. E: william.old@colorado.edu, E:stowellm@colorado.edu

Abstract

We have employed label-free quantitative proteomics of wild-type and Alzheimer's disease (AD) model mice synaptosomes to investigate proteomic changes occurring during AD progression as a prelude to analysis in humans. More than 4000 proteins were analyzed using multiple analysis tools and statistical criteria. Pathway enrichment identified numerous pathways consistent with the current AD knowledge base, including dysregulation of Glutamate Receptor Signaling, Synaptic Long Term Potentiation and Depression, Rho and Rac Signaling, Calcium Signaling, and Oxidative Phosphorylation and Mitochondrial Dysfunction. Additionally, the data demonstrate that a large number of changes occur in the proteome very early relative to the onset of both traditional disease markers such as amyloid accumulation, tau phosphorylation and cognitive dysfunction. These early changes include a number of dysregulated proteins that have novel associations with AD progression. These results reinforce the importance of mechanistic investigations in early disease progression long before the classical markers of Alzheimer's disease are observed.

Introduction

The synapse is the localized contact between nerve cells required for signal transmission and AD is considered by many to be a synaptic disease. This cell-to-cell communication is characterized by complex protein-driven molecular mechanisms including synthesis, delivery, storage, docking, fusion, neurotransmitter release and reuptake (1). Synapses can be studied by isolation of synaptosomes which contain the complete presynaptic terminal, including mitochondria and synaptic vesicles, along with

the postsynaptic membrane and the postsynaptic density. Several proteomic studies of synaptosomes have previously been performed (2–5). However, only recently has mass spectrometric analysis reached the level of technical advancement necessary for a direct and comprehensive analysis of the synaptic proteome (6). These advances in proteomics technologies allow direct and unbiased examination of protein level differences in neurodegenerative diseases and have great potential to shed new light on disease pathogenesis. Here, we employed these technical advancements in mass spectrometry for the detection of more than 4,000 synaptosomal proteins using label-free quantitative proteomics to characterize the proteome changes that occur in Alzheimer's disease (AD) model mice. Multiple structural and/or metabolic proteins have been reported to have altered expression in AD supporting a high depth quantitative proteomic analysis for target discovery (7–10).

Results

Mouse Model Characterization

The B6C3-Tg(APPswe,PSEN1dE9)85Dbo/Mmjax mouse model (Tg-AD) of Alzheimer's disease is a widely used model for AD; it contains a chimeric mouse/human amyloid precursor protein (APP)(Mo/HuAPP695swe) and human presenilin 1 (PS1-dE9); both driven by the prion protein promoter and therefore expressed in central nervous system neurons (11–15). These two insertions favor processing through the β-secretase pathway and, thus, elevate the amount of amyloid-beta (Aβ) fragments produced from the APP transgene. To validate accumulation of Aβ fragments in transgenic mice, we used

commercially available ELISA kits specific for Aβ 1-42. As shown in Fig1, both Aβ 1-42 accumulates in the brain of Tg-AD mice in an age dependent manner, supporting the choice of this mouse strain as a relevant model of AD.

Fig1. Amyloid accumulation in the APPswe/PSEN1dE9 Alzheimer's disease mouse model. (A.) Human Aβ42 was quantitated using commercially available sandwich ELISA kits at the indicated ages using both wild-type (WT) and Tg-AD (B6C3-Tg (APPswe, PSEN1dE9)85Dbo/J)) mice. Amounts of Aβ42 were normalized to total protein as determined by BCA Assay. (B.) Three, five and nine month old Tg-AD mice were chosen for high depth proteomic analysis based on the stages of Aβ load, plaque development, and cognitive decline.

Based on our Aβ accumulation data (Fig1) and upon previous characterizations of the APPswe, PSEN1dE9 biogenic mouse model which describe the timing of cognitive impairment and plaque formation (11–15), we chose to carry out a proteomic analysis of the synaptosomes of three, five, and nine month-old mice. These three age groups represent three distinct stages of AD, summarized in Fig1C. The three month-old Tg-AD age group have minimal accumulation of Aβ1-42, normal cognitive function, and complete absence of plaques. The five month-old Tg-AD mice have relatively high levels of Aβ1-42 which are accompanied by the presence of sporadic plaques although no cognitive decline has been reported. In contrast, the nine month-old Tg-AD mice represent the post-plaque and post-cognitive decline stage of AD.

Workflow

Synaptosomes from 3, 5, and 9 month-old Tg-AD and wild-type (WT) mice were isolated according to standard protocols (16). Filter Assisted Protein Preparation (FASP) was utilized to obtain pure peptides for LC-MS/MS analysis (17). Peptide samples were analyzed by online two dimensional reverse phase (RP/RP) nanoflow HPLC-MS/MS. Raw mass spectrometry data was converted to protein abundance using chromatography feature finding software MaxQuant (version 1.5.2.8) (18–20).

A total of 4,655 proteins were identified across all 18 samples using MaxQuant (18–20). All proteins categorized as potential contaminants, reverse sequence, and/or only identified by site were removed from the analysis. Biological replicates were than categorically annotated into 6 groups and proteins containing less than 2 valid values in each group were removed from the analysis, thus reducing the matrix to 3312 quantifiable proteins. (S1 Data File).

S1 Data File. Protein Quantification and Analysis.

Qualitative Analysis

A qualitative evaluation of the MS data was performed on both the WT and AD data. While biological variation is expected and accepted among replicates, due to complex and step-wise collection of RP/RP HPLC MS/MS data technical variations should be evaluated. For this analysis, we started with a hierarchical cluster analysis

(HCA) performed using complete-linkage clustering with Euclidean distance metrics of the nine WT samples (Fig2A) and the nine AD samples (Fig2B). As shown in Fig2A, the sample WT_3M_12f-C was identified as a potential outlier to other eight WT samples that are all merged into one cluster. The sub-clusters of the eight WT samples include pair-wise clustering of 3M with 5M and 5M with 9M, suggesting that age-dependent difference between the three WT age groups are negligible. In contrast, the main 2 clusters in the AD HCA (Fig2B) have a relatively short distance between them and the sub-clustering pairs include age matched AD samples, such as the pairing of AD_3M_14c-F with AD_3M_12f-AD, AD_9M_16c-CF with AD_9M_16a-D, and AD_5M_11a-C with AD_5M_11a-AB. Thus, the AD HCA suggests that differences between the age groups and, moreover, differences between the three selected stages of Alzheimer's disease will be observed.

Fig2. Qualitative Assessment of MS/MS data. A dendogram of the WT samples (A.) and the AD samples (B.) produced using Euclidean distance with complete linkage of LFQ intensity data with all invalid values removed. (B.) Histogram of absolute $\log_2$ expression values (ORANGE: WT_x – WT_average =, GREEN: 3M_x – 3M_average, BLUE: 5M_x – 5M_average, YELLOW: 9M_x – 9M_average).

To further explore the variability between replicates, we evaluated the $\log_2$ fold change of individual samples from the average (Fig2C, ORANGE: WT from the average WT, GREEN: 3M_AD from the average 3m Tg-AD, BLUE: 5M_AD from the average 5m Tg-AD, and YELLOW: 9M_AD from the average 9m Tg-AD). The expectation is that all

139 samples included in the average should have a similar shaped distribution, thus the
140 shorter and broader shape of the sample WT_3M_12f-C distribution compared to the
141 other WT samples further supports the identification of this sample as an outlier. The
142 3M_AD samples all have a similar distribution, despite the Euclidean distance of sample
143 AD_3M_14c-A from the other two 3M_AD samples (Fig2B). While the AD_5M and
144 AD_9M sample distributions are a clear reflection the short Euclidean distances observed
145 in Fig2B; in particular, the distance between AD_5M_11a-C and AD_5M_11a-AB is
146 shorter than for any other pairing and the distribution of these samples is taller and more
147 narrow than any of the other samples.

148 Together, this qualitative evaluation of the MS/MS data identifies sample
149 WT_3M_12f-C as an outlier that will be excluded from the quantitative analysis.
150 Additionally, this analysis supports that age dependent biological variability between the
151 control groups is very small. Grouping the 8 WT samples in one control group increases
152 the statistical power of the analysis, but may sacrifice age specific variations, thus further
153 evaluation of age dependent protein abundance was analyzed.

154 To determine if pooling the WT samples would be appropriate, we analyzed
155 potential age-dependent changes in the WT samples using an ANOVA multi-sample test.
156 No statistically significant proteins were identified using a loose False Discover Filter
157 (FDR, Bengamini-Hochburg) α = 0.25. Thus, to identify genes that would likely lose
158 statistical relevance if an average WT was used rather than age matched controls, we
159 applied a p-Value cut-off of 0.1 with no FDR and an absolute $\log_2$ fold change filter of 0.5.
160 We identified 73 proteins of interest (S1 Data File) that could be lost if we pooled the WT

161 samples into a single control group. However, despite these potential loses, we made the
162 decision to group all of the WT samples into a single control group.

163

164 Quantitative Assessment of Alzheimer's Disease Progression Proteome

165 R-limma (21–23) was used to perform a quantitative assessment of proteome
166 differences between the following groups: 3m Tg-AD & WT, 5m Tg-AD & WT, and 9m Tg-
167 AD & WT. Empirical Bayes statistics was used to calculate p-Values. Using a Bengamini-
168 Hochburg FDR α = 0.1, (Fig3; S1 Data File). Surprisingly, the majority of statistically
169 significant proteins identified were only significant in the pre-plaque, 3m Tg-AD, stage of
170 AD when Aβ levels are still very low. The protein expression profiles of the top most
171 dysregulated proteins ($\log_2$ FC >= |1|) are shown in Fig4. We noted that even though the
172 selection of significant proteins was dominated by the 3m Tg-AD statistical analysis, clear
173 age dependent data trends were observed; we clustered the proteins based on these
174 expression trends. This clustering shows groups of proteins that decrease (clusters 2 &
175 3) and increase (clusters 8, 9, & 10) during AD progression, that are consistently up
176 (cluster 1 & 2) or down (cluster 10 & 11), and that have stage specific protein
177 dysregulation (clusters 4, 5, 6, & 7). Eleven of the proteins of interest identified have a
178 previous association with Aβ and/or AD (Fig4 *GENE), while 73 of these high confidence
179 proteins ($\log_2$ FC >= |1|) are novel to our understanding of AD progression.

180 **Fig3. Quantitative Analysis of Age-Dependent Alzheimer's Disease.** R-limma
181 was used to calculate the p-Value and $\log_2$ fold change for the 3312 quantifiable
182 proteins using the following groupings: (A.) 3m Tg-AD & WT, (B.) 5m Tg-AD & WT,

and (C.) 9m Tg-AD & WT. A Bengamini-Hochburg FDR α = 0.1 is indicated with a solid line in each graph and the significant proteins are colored. This data and the corresponding gene names are included in Supplement File 1.

Fig4. High-Confidence Protein Expression Profiles and Clusters. Proteins were filtered using an FDR = 0.1 and an absolute FC = 1 in at least one age group. Proteins were clustered based on observable FC trend. Proteins with a previously recognized association with Aβ (24) and/or recognized by Kegg as "Alzheimer's Disease: are indicated by * next to the gene name.

STEM Analysis

As mentioned above, we observed many proteins that appeared to have a linear trend of protein expression. Time-dependent data trends can further increase confidence in the data, and analysis of these trends may even identify addition statistically significant protein changes. To further explore proteins with trending protein profiles we utilized the Short Time-series Expression Miner (STEM)(25). We used a maximum of 50 model profiles and maximum unit change of 3 ($\log_2$ FC) between time points to profile the matrix of 3312 quantifiable proteins at the three Tg-AD age groups. STEM profile enrichment identified 121 proteins that follow one of five significant profiles (S2 Data File). Fig5A-E shows these significant STEM profiles (black); the protein expression patterns that were fitted to these profiles are plotted along with the STEM profiles. Not quite half the proteins identified by STEM (58/121 proteins) were identified as significant using the empirical

Bayes statistical enrichment, while 63 new proteins were added to the list of proteins dysregulated during the progression of AD.

S2 Data File. Time-series expression analysis by STEM.

Fig5. Significant Protein Trends identified by STEM. Five protein expression profiles were identified as having more proteins fitting to the profile than would be expected by random chance. These significant profiles included three increasing profiles with 41 proteins fitting the -3, 0, 1 $\log_2$ FC profile (A.) in the 3m, 5m, and 9m age groups, respectively, 25 proteins fitting the -1, 0, 3 $\log_2$ FC profile (B.), and 16 proteins fitting the -2, -1, 1 $\log_2$ FC profile (C.). Two decreasing profiles were also identified; these were characterized by 25 proteins fitting the 3, 0, -1 $\log_2$ FC profile (D.) and 14 proteins fitting the 2, 1, -1 profile (E.) The profile summaries exported from STEM can be found in S2 Data File and the protein-to-profile assignments can be found in S2 Data File as well as in S1 Data File.

Canonical Pathway Enrichment

The benefit of adding proteins identified by STEM is demonstrated in Fig6 where Canonical Pathway Enrichment (by Ingenuity Pathway Analysis, IPA) is compared between three data filters for the 3m Tg-AD data set: a strict filter (FDR 0.1 + $\log_2$ FC >= |1|), an FDR only filter (FDR 0.1), and a STEM enriched filtered data set (FDR 0.1 + $\log_2$ FC >= |0.4|, +STEM proteins) for a select group of canonical pathways (complete list: S3 Data File). P-values for canonical pathways are calculated in IPA using a right-tailed Fisher Exact Test that considers the overlap of observed and predicted genes in a

pathway. Thus, while strict data filters will result in a high confidence gene list (Fig4), a short gene list will also produce a low confidence canonical pathway enrichment. Additionally, Fig6 & S3 Data File show that, with few exceptions, expanding the gene list to include lower confidence protein expressions identified using STEM adds to our pathway confidence (p-Value) or in other words, “what is significant becomes MORE significant”. IPA also assigns a Z-score that assesses the match of observed and predicted up/down regulation patterns. Therefore, the age-dependent FC for all proteins in the Canonical Pathway are considered. In IPA, a Z-score greater than 2 or less than -2 is considered predictive; positive Z-scores indicate activation and negative Z-scores indicate repression of the described function. As shown in Fig6, the STEM enriched protein list allows higher confidence directional predictions in comparison the FDR only filtered protein list. No predictable directionality was found in any of the enriched Canonical Pathways when the high confidence protein list (FDR 0.1, |FC|>1) was used.

S3 Data File. Canonical Pathway Enrichment.

Fig6. STEM proteins add confidence and direction to Canonical Pathway Enrichment analysis. Ingenuity Pathway Analysis (IPA) was used to analyze the 3m Tg-AD Canonical Pathway Enrichment using three different data filters: the high confidence protein list from Fig4, a standard filter (FDR = 0.1 only), and the STEM expanded FDR = 0.1 and absolute FC >= 0.4. p-Values and z-scores as calculated by IPA are shown for the top Canonical Pathways. The complete Canonical Pathway Enrichment list can be found in S3 Data File.

With this in mind we utilized the protein expression data from all proteins identified as significant (FDR = 0.1, absolute $\log_2$ FC >= 0.4) plus the STEM identified proteins to run a canonical pathway enrichment analysis. All pathways with a z-score in at least one age group are shown in Fig7. Z-scores greater than or equal to the absolute value of two are considered predictive. All dysregulated pathways, including those without a z-score, can be found in S3 Data File.

Fig7. Ingenuity Pathway Analysis (IPA) predicted direction of Canonical Pathways. IPA was used to analyze compare the directionality (z-scores) of Canonical Pathways identified enriched in the STEM expanded FDR = 0.1 and absolute FC >= 0.4 protein list. Canonical pathways with valid/non-zero z-score in at least one age group are shown here. The complete Canonical Pathway Enrichment list can be found in S3 Data File.

Discussion

The most well-known and well-studied histopathological hallmark of AD is an increase in Aβ peptide abundance and subsequent formation of amyloid plaques. Accordingly, the mouse model used in our studies should provide insights in downstream mechanisms following Aβ production. Aβ is believed to be a crucial pathogenic factor in AD development. Recent evidence indicates that the soluble-oligomeric forms of Aβ are primarily responsible for the neurodegeneration and loss of synaptic function characteristic of later stages of AD, and this soluble-Aβ hypothesis is further supported by recent clinical data on aducanumab, a human monoclonal antibody shown to reduce soluble and insoluble Aβ (26).

Surprisingly, we observed that the largest changes to the synaptosomal proteome occurred in the 3m Tg-AD mouse model where Aβ levels are relatively low, Aβ plaques are absent, and no cognitive decline is observable. While this is consistent with soluble-oligomeric forms of Aβ being primarily responsible for the pathogenesis of AD, it is notable that despite the large proteomic changes, the 3m Tg-AD mice have no observable phenotype. Very recently, a new AD phenotype has been observed: olfactory recall impairment occurs up to ten years prior to the onset of cognitive decline (27,28). This suggests that the observed proteomic changes in the 3m Tg-AD mouse may have correlated phenotypes that remain to be identified. However, it could also suggest that Aβ has a significant biological impact on the brain, even at low levels, and that compensatory mechanisms are not only active but, most importantly, are biological efficacious during the preclinical stages of AD. Although the ultimate progression of AD suggests that any early neuroprotective response to Aβ is not sustainable or is not sufficient to prevent neurotoxicity.

In typical AD progression, Aβ promotes disturbances in a number of pathways that ultimately lead to neurotoxicity. Specifically, Aβ oligomers have been reported to induce NMDA receptor activation, mitochondrial Ca2+ overload/membrane depolarization, oxidative stress and apoptotic cell death (29–32). Consistent with this pathology, we observed dysregulation in these Canonical Pathways: Glutamate Receptor Signaling, Synaptic Long Term Potentiation and Depression, Calcium Signaling, and Oxidative Phosphorylation and Mitochondrial Dysfunction (Figures 6 & 7, S3 Data File). Beyond observing dysregulation of Canonical Pathways that are consistent with what is already known about AD, we identified 73 proteins with high confidence (log_2 FC >= |1|, Fig4) that

294 are novel in our understanding of AD progression, but that are consistent with previous
295 studies. While refraining from going through all proteins/pathways, a striking example of
296 how our data supports the existing knowledge can be found by close inspection of the
297 RhoA Pathway depicted in Fig8. Specifically, our data shows an increase RhoA GEF
298 protein (ARHGEF1) and a decrease in RhoA GAP protein (RHOGAP) in the 3m Tg-AD
299 (Fig8A), consistent with activation of RhoA Signaling Pathway (Fig8B). RhoA activation,
300 as shown in Fig8A & B, leads to the activation a number of kinases whose downstream
301 activities regulate the actin cytoskeleton. ROCK, for example, is a kinase downstream of
302 RhoA that activates LIMK which in turn phosphorylates, and thus inhibits, the actin
303 severing protein, cofilin (Fig8). However, in direct opposition to the IPA's predicted state
304 of cofilin, previous observations with Aβ1-42 treatment show an increase in
305 dephosphorylated cofilin (33) and an increase of cofilin translocation into the mitochondria
306 (consistent with dephosphorylated cofilin) (34). Moreover, in AD patients, a loss or
307 shortening of dendritic spines is observed, consistent with loss of cytoskeletal stability.
308 Previous studies have also shown that Aβ1-42 treatment of hippocampal neurons induced
309 increased activity in Rac1, Cdc42, and PAK1 (33), which, like RhoA, are also involved in
310 activation of LIMK and the phosphorylation of cofilin. Together, this data suggests that Aβ
311 either inhibits phosphorylation or promotes dephosphorylation of cofilin and that activation
312 of upstream activators of LIMK may be a compensation mechanism for the increase in
313 dephosphorylated cofilin. Potential mechanisms of Aβ's regulatory role on cofilin
314 phosphorylation and dephosphorylation are illustrated in Fig9A.

315 **Fig8. RhoA Signaling Pathway activation in early AD**. (A.) Canonical Pathway
316 enrichment analysis identified RhoA as activated in the 3m Tg-AD. (B.) The $\log_2$

317 FC of eight proteins within the RhoA Signaling Pathway were used to calculate the
318 z-score and the predicted directionality of RhoA Signaling. (C.) These molecules
319 are colored red (up-regulated) or blue (down-regulated) in a schematic of the RhoA
320 Signaling pathway in the 3m Tg-AD. (D.) IPA's Molecular Activation Predictor
321 illustrates the predicted outcome of the 3m Tg-AD protein abundance changes.
322 (Red = activated; Blue = inhibited; Yellow = inconsistent with state of downstream
323 molecule)

324 **Fig9. Proposed Aβ's impact on Cofilin Phosphorylation and actin**
325 **stabilization.** Our study, in concert with previous studies, implicates Aβ
326 involvement in the activation of a number of molecules upstream of Cofilin
327 regulation and actin stabilization. (Red = activated; Blue = inhibited; Yellow =
328 inconsistent with state of downstream molecule)

329

330 Compensation for Aβ induced dysregulation of cofilin-actin dynamics would be
331 required for sustained neural function and survival. Cofilin-actin regulation is critical for
332 morphogenesis and the structural dynamics of neural spines and has been strongly
333 implicated in synaptic trafficking of AMPA receptors during Synaptic Potentiation and
334 Depression (35,36). In the 3m Tg-AD, we do not see a significant difference in the number
335 of AMPA receptors (GRIA). However, we assume there is successful compensatory
336 stabilization of actin filaments through the RhoA Signaling Pathway.

337 The RhoA Signaling Pathway represents only one of many pathways that were
338 found to be dysregulated in the pre-clinical 3m Tg-AD model. Understanding how these

pathways take part in the response to Aβ may lead to new therapeutic avenues for AD. Additionally, recognition of the early dysregulation of these pathways may help identify new, pre-clinical, phenotypes for AD.

Methods

Mice

Mice used in the experiments were housed in accordance with protocols approved by the Institutional Animal Care and Use Committee at University of Colorado and all experiments were conducted according to the NIH Guide for the Care and Use of Laboratory Animals. The B6C3-Tg(APPswe, PSEN1dE9)85Dbo/J) breeding pair was obtained from The Jackson Laboratory (stock number 004462). Colony was maintained using +/+ sibling x Hemi zygote. Ear punches were taken at approximately 10 days old and PCR identification was performed to identify AD transgenic mice and the non-transgenic littermate controls. The AD transgenic mice and the non-transgenic littermate controls of the same sex were housed in individual ventilated cages, with a maximum of five mice per cage. Female B6C3-Tg(APPswe, PSEN1dE9)85Dbo/J) transgenic mice at various ages (3, 5, and 9 months) and their age-matched, non-transgenic littermate controls (wild type, WT) were used in this study. For quality control purposes tail clips were taken at the time of death and a second genotyping was performed to confirm the first.

ELISA

Hemi-brain samples were analyzed for human Aβ 1-40 and 1-42 using commercially available ELISA kits (Life Technologies: KHB3481 & KHB3441) according

to manufacturer's instruction. Amounts of Aβ were normalized to total protein as determined by BCA assay (Pierce #23225).

Synaptosome Isolation

All mice were sacrificed at the age indicated. Synaptosomes were isolated as previously described with minor modifications (16). The whole brain was dissected from one mouse and homogenized with 20 strokes in 2 mL of complete sucrose buffer (0.32 M Sucrose; 2 mM EGTA; 2 mM EDTA; 10 mM HEPES (pH 7.4), 1x Protease Inhibitor Cocktail: cOmplete, EDTA-free (Roche 05 056 489 001), 1mM Na_3VO_4 (Sodium Vanadate), 1mM $Na_4O_7P_2$ (Sodium Pyrophosphate). Centrifuged at 800 x g for 10 minutes at 4°C to pellet the membrane fragments and nuclei and collect supernatant (S1) in 15 mL conical tubes then fast frozen in liquid nitrogen and then stored at 70°C until all mouse brain samples for were collected. To minimize technical variability, synaptosomal preparation was performed in age-matched batches. All batch purifications were performed with the same stock buffers within 24 hours of each other. To prepare purified synaptosomes the S1 samples were thawed on ice, centrifuged at 800 x g for 10 minutes at 4°C and collect supernatant (S1') in high-speed polycarbonate tubes. S1' fractions were then centrifuged at 10,000 x g for 15 minutes at 4°C to obtain a pellet (P2) containing synaptosomes contaminated with mitochondria and microsomes. P2 was suspended in 500 µl of Complete Sucrose Buffer, vortexed thoroughly then loaded on a sucrose gradient (from bottom to top): 1.18 M – 1.0 M – 0.85 M (all prepared in 10 mM HEPES, pH 7.4, 2 mM EDTA, 2 mM EGTA) prior to centrifuging at 82,500 x g for 1 hour at 4°C. Pure synaptosomes were collected from the interface between 1.0 M and 1.18 M, washed by adding ~3X volume of Complete Sucrose Buffer and centrifuged at 10,000 x g for 15

minutes at 4°C prior to re-suspending in Complete Sucrose Buffer and measuring of protein concentration using a micro BCA Protein Assay (Pierce 22660) according to manufacturer's instructions. Pure synaptosomes were divided into 50 µg aliquots and stored at -80°C.

Peptide Preparation

Peptide preparation was performed by the Filter Assisted Sample Preparation (FASP) method as described (17). Briefly, to extract membrane proteins in the synaptosome samples, a 0.3% concentration of Triton X-100 was used to solubilize 50 µg of purified synaptosomes. The sample was then washed with fresh 8 M and 2 M Urea Buffer in a 30 kDa filter (Millipore UFC 503024); the proteins were reduced (10 mM TCEP) and alkylated (25 mM IA) and treated with trypsin (Promega #V5113; 1:100 or 0.05 µg of trypsin per 50 µg sample) overnight in the spin filter. The resulting peptides were desalted in C-18 spin columns (Pierce 89870) according to the manufacturer's instructions. The peptide concentration was estimated using a NanoDrop 2000 and Bovine Serum Albumin as reference (mass extinction coefficient of 6.7 at 280 nm) resulting in 6-7 µg of peptide per sample. The peptide was then immediately lyophilized for 2 hours, and stored at -80°C.

RP-RP MS/MS

The peptides were separated by liquid chromatography using a nanoAcquity UPLC system (Waters) coupled to a LTQ Orbitrap mass spectrometer (Thermo Fisher Scientific). Peptide mixtures (2 µg) were loaded onto a 300-µm × 50-mm XBridge C18, 130-Å, 5-µm column maintained at pH 10.0, eluting peptides in six fractions

corresponding to 10%, 15%, 20%, 30%, 40%, and 60% buffer B1 (buffer A1: 20 mM ammonium formate, pH 10.0; and buffer B1: 100% acetonitrile). Steps were eluted from the high pH column at 20 µl/min onto a 180-µm × 20-mm C18, 100-Å, 5-µm trap column, which was then switched in-line with the analytical column and eluted as in the 1D method. For 1D analysis, a BEH C18 reversed phase column (25 cm × 75 µm i.d., 1.7 µm, 100 Å; Waters) was used for the analytical separation using a linear gradient from 90% buffer A2 (0.1% formic acid) to 40% buffer B2 (0.1% formic acid and 80% acetonitrile) over 60 min at a flow rate of 300 nL/min.

MS/MS data were collected by an enabling monoisotopic precursor and charge selection settings. Ions with unassigned charge state were excluded. For each mass spectrometry scan, the 10 most intense ions were targeted with dynamic exclusion 30 s, 1 D exclusion width, and repeat count equal to 1. The maximum injection time for Orbitrap parent scans was 500 ms, allowing 1 microscan and automatic gain control of 106. The maximal injection time for the LTQ MS/MS was 250 ms, with 1 microscan and automatic gain control of 104. The normalized collision energy was 35%, with activation Q of 0.25 for 30 ms.

Data Analysis

The raw MS/MS data from all samples were analyzed by MaxQuant (37)(version 1.5.2.8). Andromeda (38), a probabilistic search engine incorporated into the MaxQuant framework was used to search the peak list against the Uniprot_MOUSE database (UniProtKB release 2016_098, entries: 82,200). Common contaminants were added to this database. The search included cysteine carbamidomethylation as a fixed modification

and N-terminal acetylation and methionine oxidation as variable modifications. The false discovery rate (FDR) was set to 0.01 for both peptide and protein identifications. Enzyme specificity was set to trypsin allowing N-terminal cleavage to proline. Two miscleavages were allowed, and a minimum of seven amino acids per identified peptide were required. Peptide identification was based on a search with an initial mass deviation of the precursor ion (ITMS) of up to 0.5 Da, and the allowed fragment mass deviation (FTMS) was set to 20 ppm. Razor peptides were used for quantification; unmodified or with the modifications specified above. To match identifications across different replicates and adjacent fractions, the “match between runs” option in MaxQuant was enabled within a matching time window of 0.7 min.

Bioinformatics analysis was done with Perseus (39)(version 1.4.1.3) tools available in the MaxQuant environment. The proteins only identified by site, from the reverse database, and contaminant proteins were removed from the matrix. Categorical annotation by age and type was performed resulting in 6 groups: AD_3M, AD_5M, AD_9M, WT_3M, WT_5M, & WT_9M, with an n=3 in each group. The protein matrix was reduced to those identifications with at least one valid observation in each group. A multiple-sample test was run between WT_3M, WT_5M, & WT_9M using a Bengamini-Hochburg FDR=0.25 (7 significant) and these proteins were removed from the matrix. The 9 WT samples were then pooled into one WT group and the data was exported for further analysis with R version 3.3.1 (2016-06-21) and the package limma (21,23) (version 3.28.14). Limma was then used to calculate the $\log_2$ fold change and the empirical Bayes p-Value between the following groups: AD_9m & WT, AD_5m & WT, AD_3m & WT, WT_9m & WT, WT_5m & WT, and WT_3m & WT.

Acknowledgements

References

1. Purves D, Augustine GJ, Fitzpatrick D, Hall WC, LaMantia A-S, McNamara JO, et al., editors. Neuroscience. 3rd ed. Sunderland, MA: Sinaur Associates, Inc; 2004. 832 p.

2. Boyd-Kimball D, Castegna A, Sultana R, Poon HF, Petroze R, Lynn BC, et al. Proteomic identification of proteins oxidized by Abeta(1-42) in synaptosomes: implications for Alzheimer's disease. Brain Res. 2005 May 24;1044(2):206–15.

3. Schrimpf SP, Meskenaite V, Brunner E, Rutishauser D, Walther P, Eng J, et al. Proteomic analysis of synaptosomes using isotope-coded affinity tags and mass spectrometry. PROTEOMICS. 2005;5(10):2531–2541.

4. Witzmann FA, Arnold RJ, Bai F, Hrncirova P, Kimpel MW, Mechref YS, et al. A proteomic survey of rat cerebral cortical synaptosomes. Proteomics. 2005 May;5(8):2177–201.

5. Bai F, Witzmann FA. Synaptosome proteomics. Subcell Biochem. 2007;43:77–98.

6. Siu SO, Lam MPY, Lau E, Kong RPW, Lee SMY, Chu IK. Fully automatable two-dimensional reversed-phase capillary liquid chromatography with online tandem mass spectrometry for shotgun proteomics. Proteomics. 2011 Jun;11(11):2308–19.

7. Walsh DM, Klyubin I, Fadeeva JV, Cullen WK, Anwyl R, Wolfe MS, et al. Naturally secreted oligomers of amyloid β protein potently inhibit hippocampal long-term potentiation in vivo. Nature. 2002 Apr 4;416(6880):535–9.

8. Harmeier A, Wozny C, Rost BR, Munter L-M, Hua H, Georgiev O, et al. Role of Amyloid-β Glycine 33 in Oligomerization, Toxicity, and Neuronal Plasticity. J Neurosci. 2009 Jun 10;29(23):7582–90.

9. Terry RD, Masliah E, Salmon DP, Butters N, DeTeresa R, Hill R, et al. Physical basis of cognitive alterations in Alzheimer's disease: synapse loss is the major correlate of cognitive impairment. Ann Neurol. 1991 Oct;30(4):572–80.

10. Kim SI, Voshol H, van Oostrum J, Hastings TG, Cascio M, Glucksman MJ. Neuroproteomics: expression profiling of the brain's proteomes in health and disease. Neurochem Res. 2004 Jun;29(6):1317–31.

11. Reiserer RS, Harrison FE, Syverud DC, McDonald MP. Impaired spatial learning in the APPSwe + PSEN1DeltaE9 bigenic mouse model of Alzheimer's disease. Genes Brain Behav. 2007 Feb;6(1):54–65.

12. Spires TL, Hyman BT. Transgenic models of Alzheimer's disease: learning from animals. NeuroRx J Am Soc Exp Neurother. 2005 Jul;2(3):423–37.

13. Harrison FE, Hosseini AH, McDonald MP, May JM. Vitamin C reduces spatial learning deficits in middle-aged and very old APP/PSEN1 transgenic and wild-type mice. Pharmacol Biochem Behav. 2009 Oct;93(4):443–50.

14. Garcia-Alloza M, Robbins EM, Zhang-Nunes SX, Purcell SM, Betensky RA, Raju S, et al. Characterization of amyloid deposition in the APPswe/PS1dE9 mouse model of Alzheimer disease. Neurobiol Dis. 2006 Dec;24(3):516–24.

15. Takeda S, Hashimoto T, Roe AD, Hori Y, Spires-Jones TL, Hyman BT. Brain interstitial oligomeric amyloid β increases with age and is resistant to clearance from brain in a mouse model of Alzheimer's disease. FASEB J Off Publ Fed Am Soc Exp Biol. 2013 Aug;27(8):3239–48.

16. Hajós F. An improved method for the preparation of synaptosomal fractions in high purity. Brain Res. 1975 Aug 15;93(3):485–9.

17. Wiśniewski JR, Zougman A, Nagaraj N, Mann M. Universal sample preparation method for proteome analysis. Nat Methods. 2009 May;6(5):359–62.

18. Tyanova S, Temu T, Carlson A, Sinitcyn P, Mann M, Cox J. Visualization of LC-MS/MS proteomics data in MaxQuant. PROTEOMICS. 2015 Apr 1;15(8):1453–6.

19. Cox J, Hein MY, Luber CA, Paron I, Nagaraj N, Mann M. Accurate Proteome-wide Label-free Quantification by Delayed Normalization and Maximal Peptide Ratio Extraction, Termed MaxLFQ. Mol Cell Proteomics MCP. 2014 Sep;13(9):2513–26.

20. Schaab C, Geiger T, Stoehr G, Cox J, Mann M. Analysis of High Accuracy, Quantitative Proteomics Data in the MaxQB Database. Mol Cell Proteomics MCP [Internet]. 2012 Mar [cited 2015 Nov 6];11(3). Available from: http://www.ncbi.nlm.nih.gov/pmc/articles/PMC3316731/

21. Ritchie ME, Phipson B, Wu D, Hu Y, Law CW, Shi W, et al. limma powers differential expression analyses for RNA-sequencing and microarray studies. Nucleic Acids Res. 2015 Apr 20;43(7):e47.

22. Phipson B, Lee S, Majewski IJ, Alexander WS, Smyth GK. Robust hyperparameter estimation protects against hypervariable genes and improves power to detect differential expression. Ann Appl Stat. 2016 Jun;10(2):946–63.

23. Smyth GK. Linear models and empirical bayes methods for assessing differential expression in microarray experiments. Stat Appl Genet Mol Biol. 2004;3:Article3.

24. Campion D, Pottier C, Nicolas G, Le Guennec K, Rovelet-Lecrux A. Alzheimer disease: modeling an Aβ-centered biological network. Mol Psychiatry. 2016 Jul;21(7):861–71.

25. Ernst J, Bar-Joseph Z. STEM: a tool for the analysis of short time series gene expression data. BMC Bioinformatics. 2006 Apr 5;7:191.

26. Sevigny J, Chiao P, Bussière T, Weinreb PH, Williams L, Maier M, et al. The antibody aducanumab reduces Aβ plaques in Alzheimer's disease. Nature. 2016 Sep 1;537(7618):50–6.

27. Morgan CD, Murphy C. Individuals at risk for Alzheimer's disease show differential patterns of ERP brain activation during odor identification. Behav Brain Funct. 2012 Jul 31;8(1):37.

28. Attems J, Walker L, Jellinger KA. Olfactory bulb involvement in neurodegenerative diseases. Acta Neuropathol (Berl). 2014 Apr;127(4):459–75.

29. Alberdi E, Sánchez-Gómez MV, Cavaliere F, Pérez-Samartín A, Zugaza JL, Trullas R, et al. Amyloid beta oligomers induce Ca2+ dysregulation and neuronal death through activation of ionotropic glutamate receptors. Cell Calcium. 2010 Mar;47(3):264–72.

30. Bieschke J, Herbst M, Wiglenda T, Friedrich RP, Boeddrich A, Schiele F, et al. Small-molecule conversion of toxic oligomers to nontoxic β-sheet-rich amyloid fibrils. Nat Chem Biol. 2011 Nov 20;8(1):93–101.

31. Shelat PB, Chalimoniuk M, Wang J-H, Strosznajder JB, Lee JC, Sun AY, et al. Amyloid beta peptide and NMDA induce ROS from NADPH oxidase and AA release from cytosolic phospholipase A2 in cortical neurons. J Neurochem. 2008 Jul 1;106(1):45–55.

32. Mattson MP, Cheng B, Davis D, Bryant K, Lieberburg I, Rydel RE. beta-Amyloid peptides destabilize calcium homeostasis and render human cortical neurons vulnerable to excitotoxicity. J Neurosci Off J Soc Neurosci. 1992 Feb;12(2):376–89.

33. Mendoza-Naranjo A, Contreras-Vallejos E, Henriquez DR, Otth C, Bamburg JR, Maccioni RB, et al. Fibrillar amyloid-β1-42 modifies actin organization affecting the cofilin phosphorylation state: a role for Rac1/cdc42 effector proteins and the slingshot phosphatase. J Alzheimers Dis JAD. 2012;29(1):63–77.

34. Woo JA, Boggess T, Uhlar C, Wang X, Khan H, Cappos G, et al. RanBP9 at the intersection between cofilin and Aβ pathologies: rescue of neurodegenerative changes by RanBP9 reduction. Cell Death Dis. 2015 Mar 5;6:1676.

35. Yuen EY, Yan Z. Dopamine D4 Receptors Regulate AMPA Receptor Trafficking and Glutamatergic Transmission in GABAergic Interneurons of Prefrontal Cortex. J Neurosci Off J Soc Neurosci. 2009 Jan 14;29(2):550–62.

36. Correia SS, Bassani S, Brown TC, Lisé M-F, Backos DS, El-Husseini A, et al. Motor protein–dependent transport of AMPA receptors into spines during long-term potentiation. Nat Neurosci. 2008 Apr;11(4):457–66.

552 37. Cox J, Mann M. MaxQuant enables high peptide identification rates, individualized p.p.b.-
553 range mass accuracies and proteome-wide protein quantification. Nat Biotechnol. 2008
554 Dec;26(12):1367–72.

555 38. Cox J, Neuhauser N, Michalski A, Scheltema RA, Olsen JV, Mann M. Andromeda: A Peptide
556 Search Engine Integrated into the MaxQuant Environment. J Proteome Res. 2011 Apr
557 1;10(4):1794–805.

558 39. Cox J, Mann M. 1D and 2D annotation enrichment: a statistical method integrating
559 quantitative proteomics with complementary high-throughput data. BMC Bioinformatics.
560 2012;13 Suppl 16:S12.

561

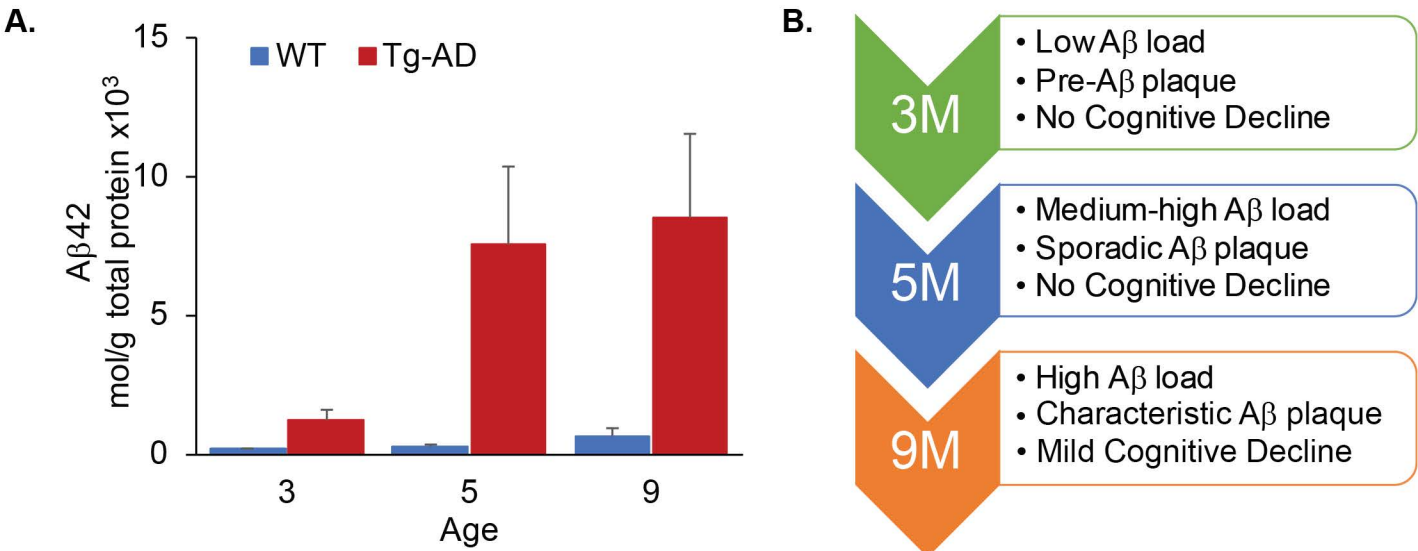
A.
WT
Tg-AD
Aβ42
mol/g total protein x10³
15
10
5
0
3
5
9
Age
(months)
B.
3M
• Low Aβ load
• Pre-Aβ plaque
• No Cognitive Decline
5M
• Medium-high Aβ load
• Sporadic Aβ plaque
• No Cognitive Decline
9M
• High Aβ load
• Characteristic Aβ plaque
• Mild Cognitive Decline

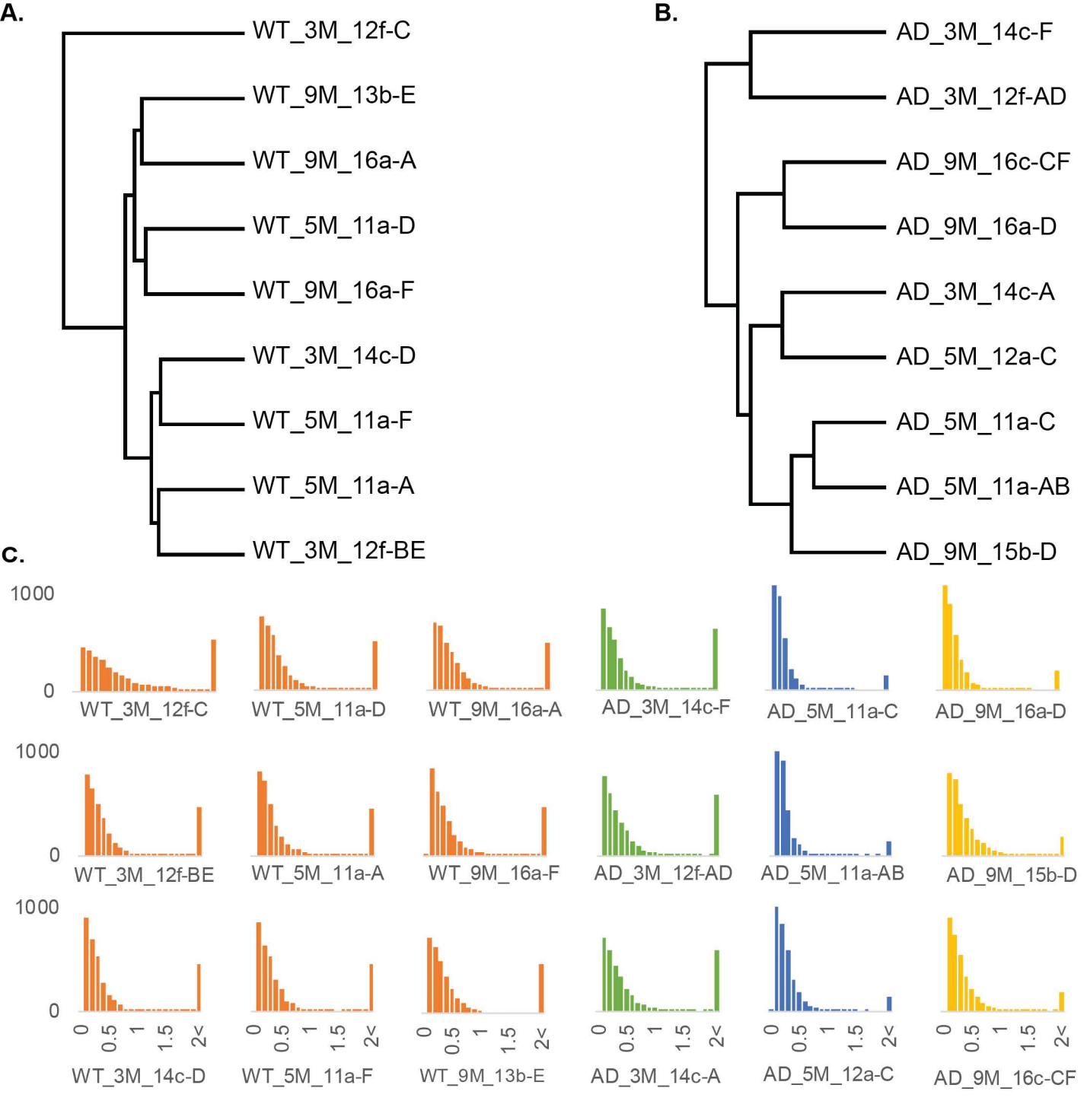
A.
WT_3M_12f-C
WT_9M_13b-E
WT_9M_16a-A
WT_5M_11a-D
WT_9M_16a-F
WT_3M_14c-D
WT_5M_11a-F
WT_5M_11a-A
WT_3M_12f-BE
B.
AD_3M_14c-F
AD_3M_12f-AD
AD_9M_16c-CF
AD_9M_16a-D
AD_3M_14c-A
AD_5M_12a-C
AD_5M_11a-C
AD_5M_11a-AB
AD_9M_15b-D
C.
1000
0
WT_3M_12f-C
WT_5M_11a-D
WT_9M_16a-A
AD_3M_14c-F
AD_5M_11a-C
AD_9M_16a-D
WT_3M_12f-BE
WT_5M_11a-A
WT_9M_16a-F
AD_3M_12f-AD
AD_5M_11a-AB
AD_9M_15b-D
0
0.5
1
1.5
2<
WT_3M_14c-D
WT_5M_11a-F
WT_9M_13b-E
AD_3M_14c-A
AD_5M_12a-C
AD_9M_16c-CF

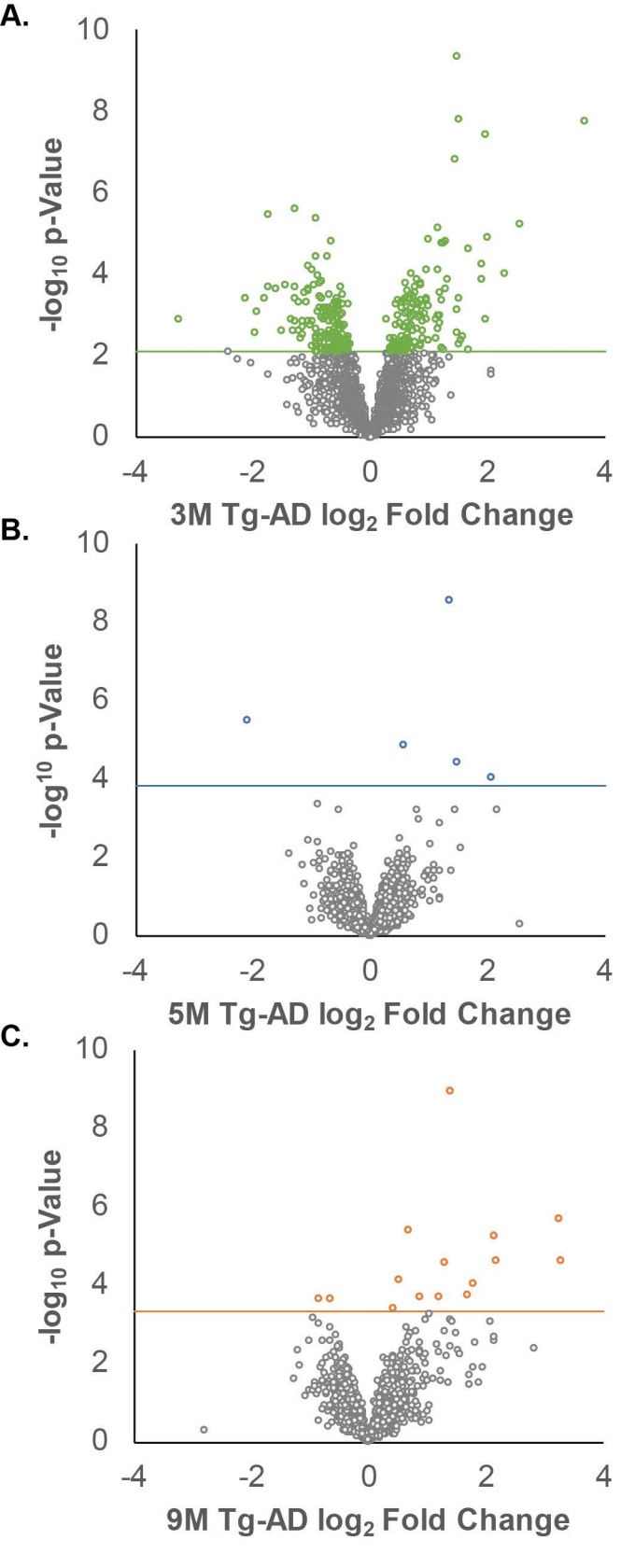
A.
10
8
6
4
2
0
-log10 p-Value
-4
-2
0
2
4
3M Tg-AD log2 Fold Change
B.
10
8
6
4
2
0
-log10 p-Value
-4
-2
0
2
4
5M Tg-AD log2 Fold Change
C.
10
8
6
4
2
0
-log10 p-Value
-4
-2
0
2
4
9M Tg-AD log2 Fold Change

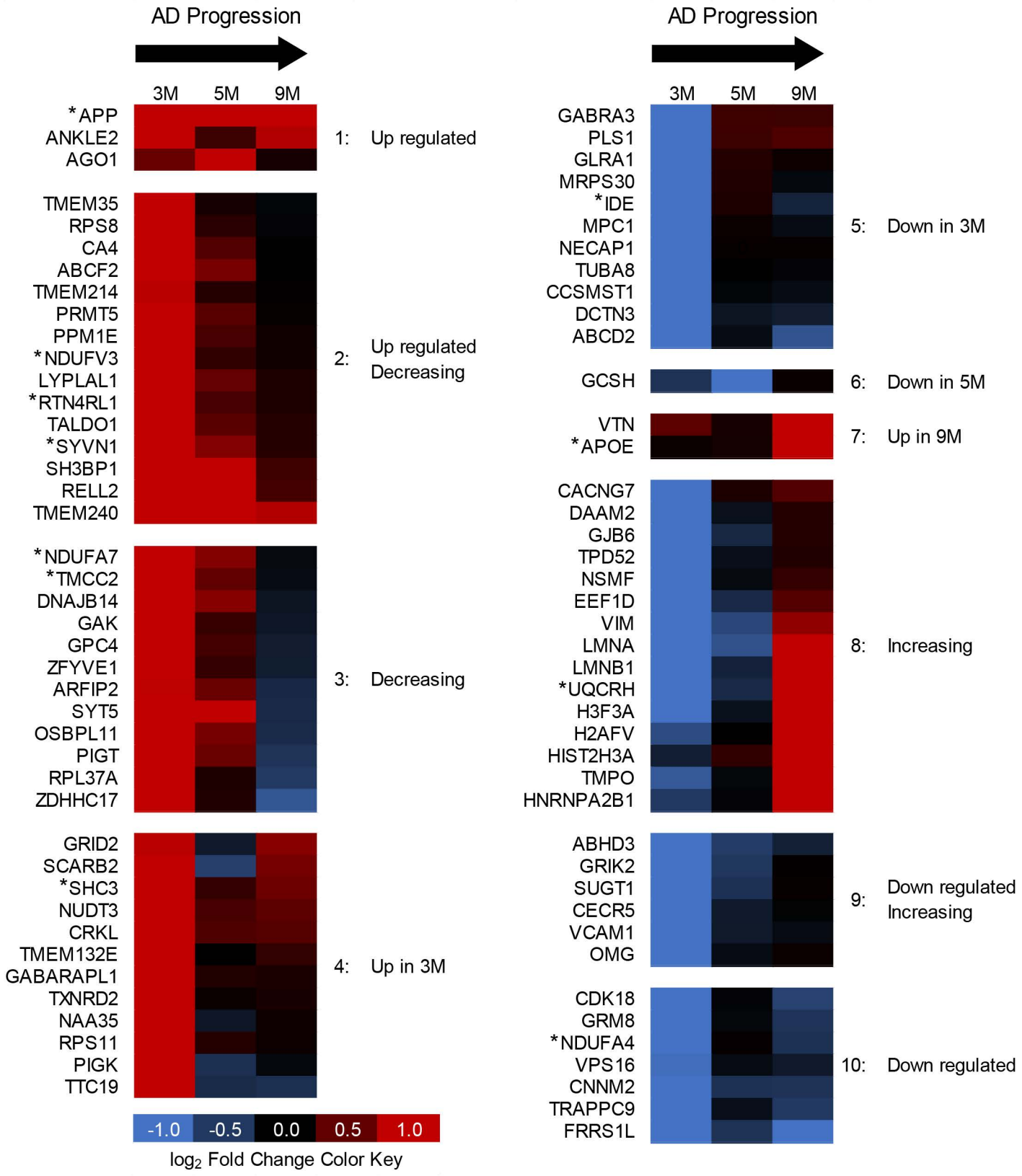
AD Progression
3M
5M
9M
*APP
ANKLE2
AGO1
1: Up regulated
TMEM35
RPS8
CA4
ABCF2
TMEM214
PRMT5
PPM1E
*NDUFV3
LYPLAL1
*RTN4RL1
TALDO1
*SYVN1
SH3BP1
RELL2
TMEM240
2: Up regulated Decreasing
*NDUFA7
*TMCC2
DNAJB14
GAK
GPC4
ZFYVE1
ARFIP2
SYT5
OSBPL11
PIGT
RPL37A
ZDHHC17
3: Decreasing
GRID2
SCARB2
*SHC3
NUDT3
CRKL
TMEM132E
GABARAPL1
TXNRD2
NAA35
RPS11
PIGK
TTC19
4: Up in 3M
-1.0
-0.5
0.0
0.5
1.0
log2 Fold Change Color Key
AD Progression
3M
5M
9M
GABRA3
PLS1
GLRA1
MRPS30
*IDE
MPC1
NECAP1
TUBA8
CCSMST1
DCTN3
ABCD2
5: Down in 3M
GCSH
6: Down in 5M
VTN
*APOE
7: Up in 9M
CACNG7
DAAM2
GJB6
TPD52
NSMF
EEF1D
VIM
LMNA
LMNB1
*UQCRH
H3F3A
H2AFV
HIST2H3A
TMPO
HNRNPA2B1
8: Increasing
ABHD3
GRIK2
SUGT1
CECR5
VCAM1
OMG
9: Down regulated Increasing
CDK18
GRM8
*NDUFA4
VPS16
CNNM2
TRAPPC9
FRRS1L
10: Down regulated

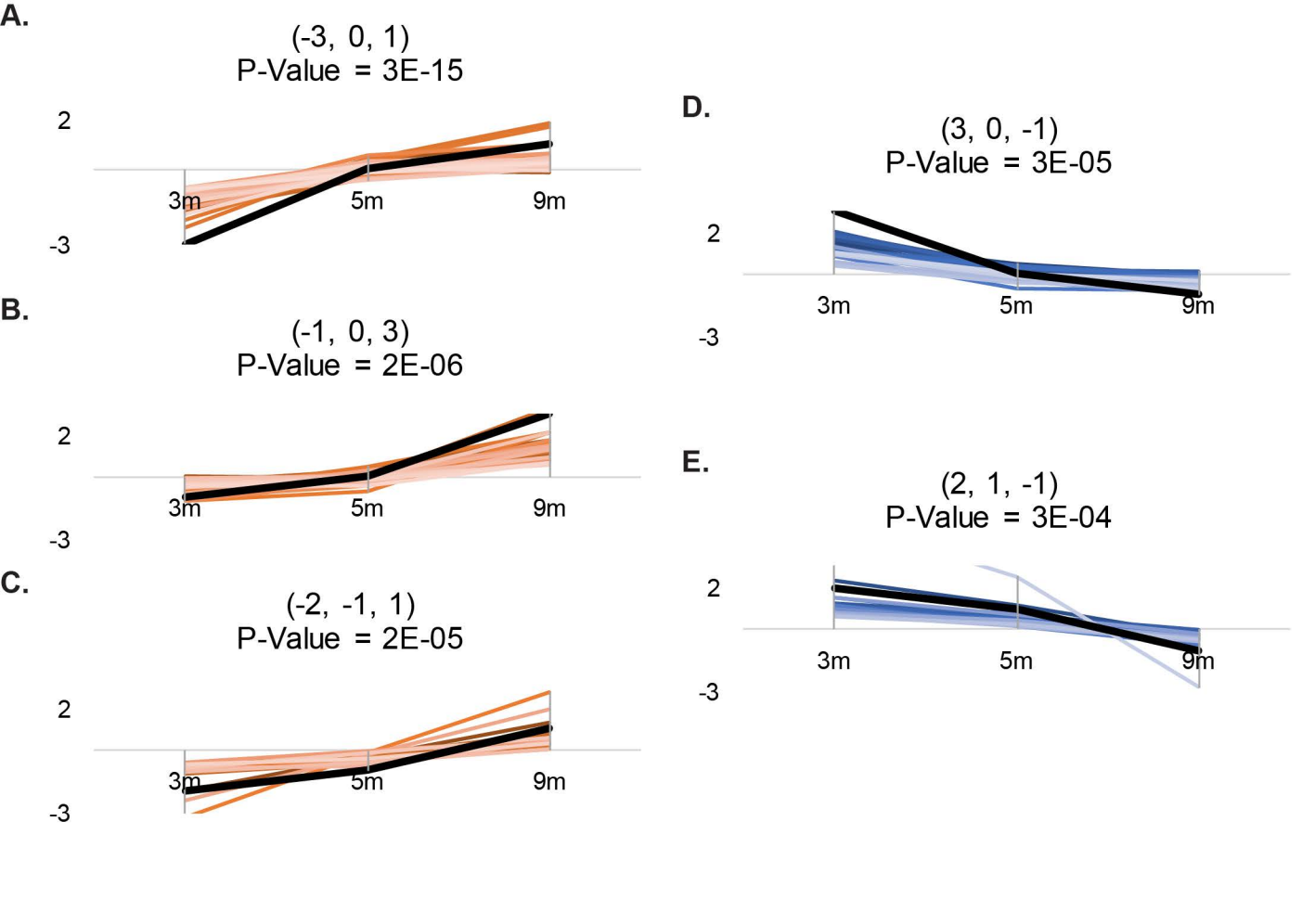
A.
(-3, 0, 1)
P-Value = 3E-15
2
-3
3m
5m
9m
B.
(-1, 0, 3)
P-Value = 2E-06
2
-3
3m
5m
9m
C.
(-2, -1, 1)
P-Value = 2E-05
2
-3
3m
5m
9m
D.
(3, 0, -1)
P-Value = 3E-05
2
-3
3m
5m
9m
E.
(2, 1, -1)
P-Value = 3E-04
2
-3
3m
5m
9m

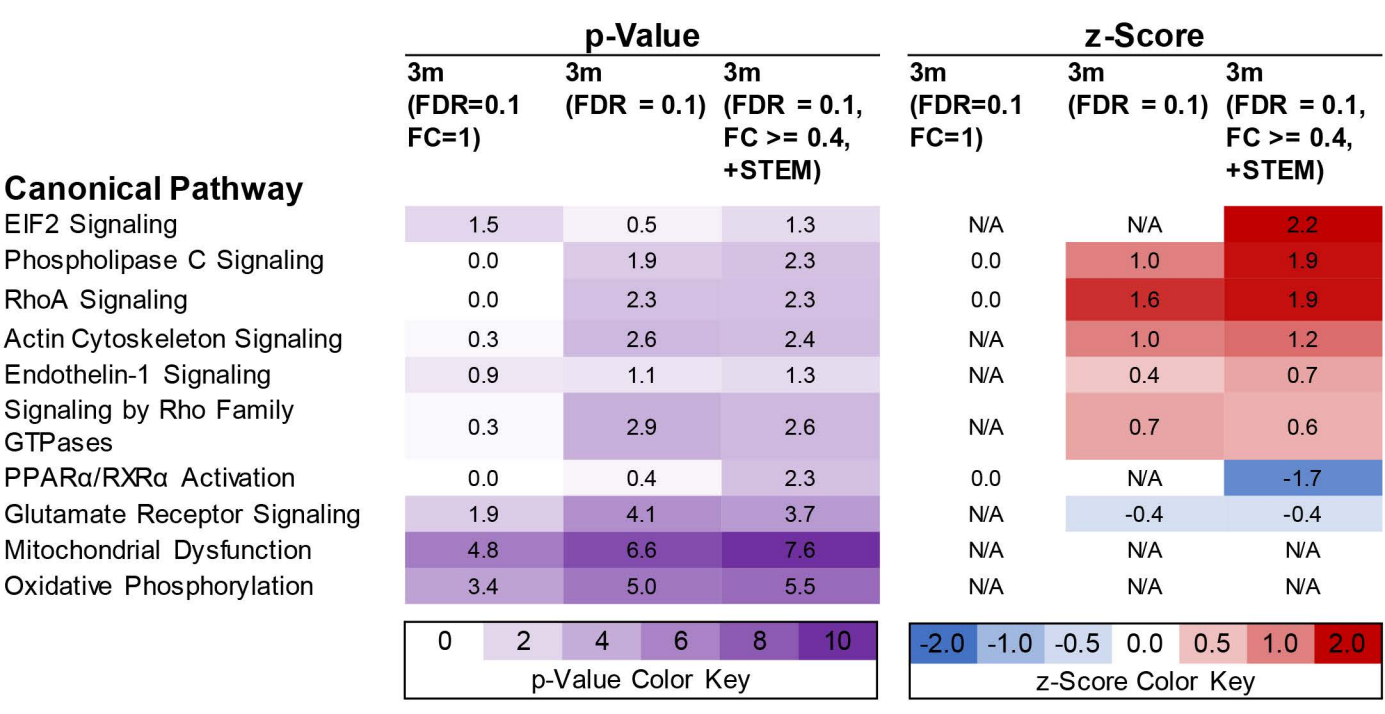
p-Value
z-Score
3m (FDR=0.1 FC=1)
3m (FDR = 0.1)
3m (FDR = 0.1, FC >= 0.4, +STEM)
3m (FDR=0.1 FC=1)
3m (FDR = 0.1)
3m (FDR = 0.1, FC >= 0.4, +STEM)
Canonical Pathway
EIF2 Signaling 1.5 0.5 1.3 N/A N/A 2.2
Phospholipase C Signaling 0.0 1.9 2.3 0.0 1.0 1.9
RhoA Signaling 0.0 2.3 2.3 0.0 1.6 1.9
Actin Cytoskeleton Signaling 0.3 2.6 2.4 N/A 1.0 1.2
Endothelin-1 Signaling 0.9 1.1 1.3 N/A 0.4 0.7
Signaling by Rho Family GTPases 0.3 2.9 2.6 N/A 0.7 0.6
PPARα/RXRα Activation 0.0 0.4 2.3 0.0 N/A -1.7
Glutamate Receptor Signaling 1.9 4.1 3.7 N/A -0.4 -0.4
Mitochondrial Dysfunction 4.8 6.6 7.6 N/A N/A N/A
Oxidative Phosphorylation 3.4 5.0 5.5 N/A N/A N/A
0 2 4 6 8 10
p-Value Color Key
-2.0 -1.0 -0.5 0.0 0.5 1.0 2.0
z-Score Color Key

Canonical Pathway	STEM enriched 3m	5m	9m
RhoA Signaling	1.9	0.8	N/A
Phospholipase C Signaling	1.9	2.4	1.3
Actin Cytoskeleton Signaling	1.2	0.3	1.7
EIF2 Signaling	2.2	1.3	-1.3
α-Adrenergic Signaling	0.8	1.6	-0.4
Thrombin Signaling	0.4	1.1	-0.4
Signaling by Rho Family GTPases	0.6	-0.3	1.6
CREB Signaling in Neurons	0.7	-0.7	1.1
NRF2-mediated Oxidative Stress Response	1.3	-0.4	0.4
IL-1 Signaling	1.0	-1.0	N/A
Synaptic Long Term Potentiation	0.8	-0.4	-0.4
Synaptic Long Term Depression	0.4	-1.1	-1.3
G Beta Gamma Signaling	1.3	-0.4	-1.0
Huntington's Disease Signaling	1.0	0.0	-1.0
Endothelin-1 Signaling	0.7	0.0	-1.3
fMLP Signaling in Neutrophils	1.0	N/A	N/A
Ephrin Receptor Signaling	0.8	0.0	0.0
Fcγ Receptor-mediated Phagocytosis in Macrophages and Monocytes	0.4	N/A	N/A
Integrin Signaling	-0.3	0.8	1.1
Calcium Signaling	0.0	0.4	1.6
Insulin Receptor Signaling	-0.4	1.1	-0.4
RhoGDI Signaling	-0.7	0.4	N/A
PPARα/RXRα Activation	-1.7	-1.0	2.1
Glutamate Receptor Signaling	-0.4	-1.3	1.0
Apoptosis Signaling	-1.0	-1.0	1.0
LPS/IL-1 Mediated Inhibition of RXR Function	0.0	N/A	-1.0
Gαi Signaling	-1.3	-0.4	-2.0

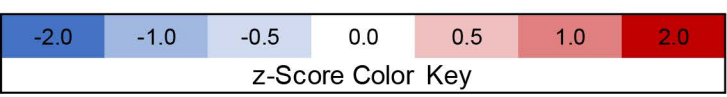

A.

Canonical Pathway	z-Score 3M	5M	9M
RhoA Signaling	1.9	0.8	N/A

B.

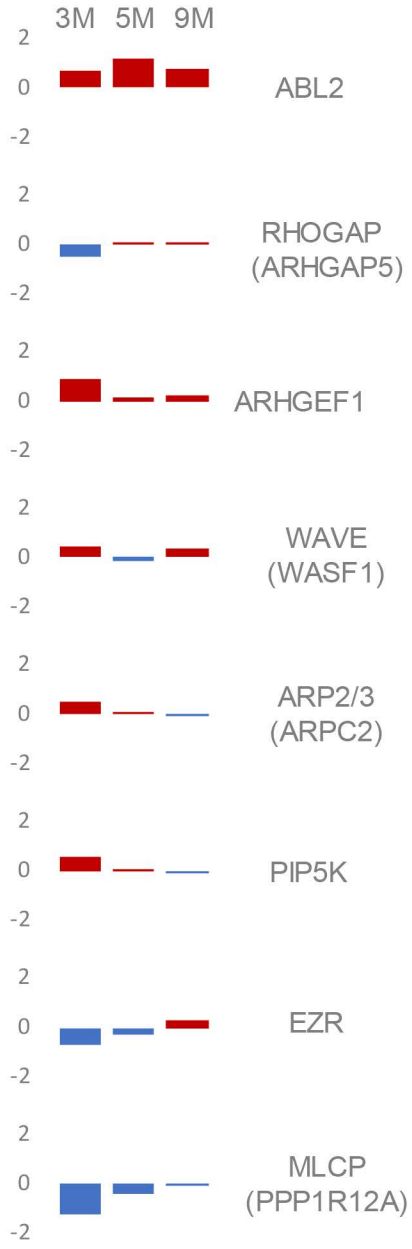

C. 3m Tg-AD

Up-regulated
Down-regulated

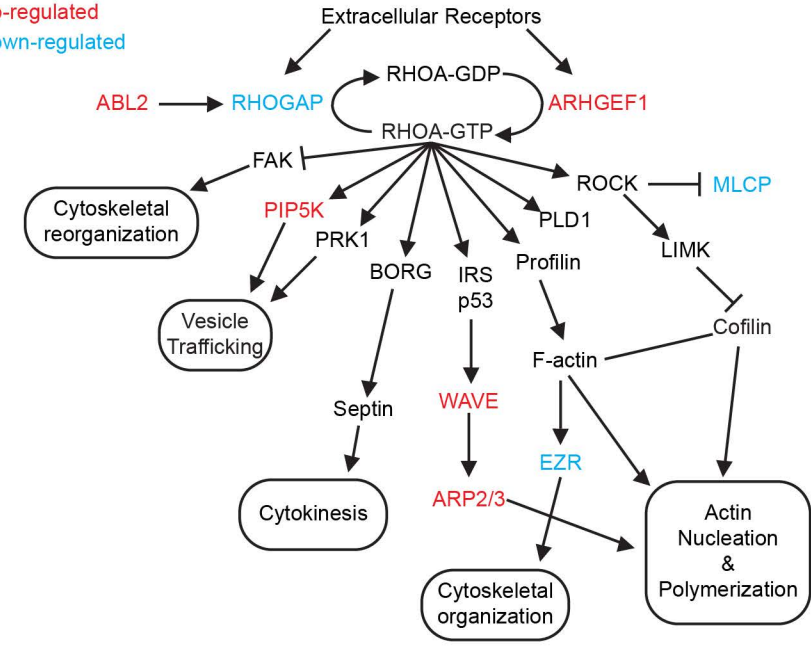

D. 3m Tg-AD IPA Molecule Activation Predictor

Activated
Inhibited
Inconsistent with state of downstream molecule

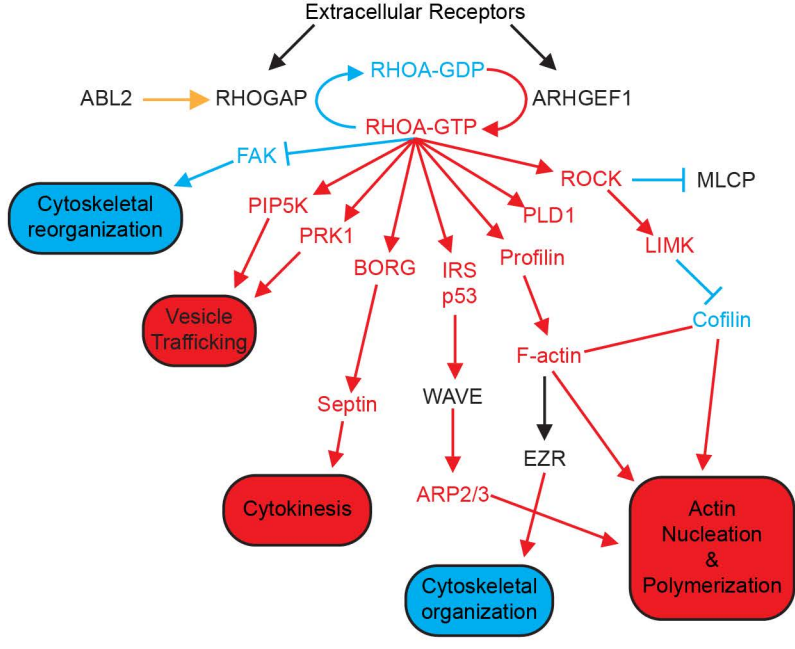

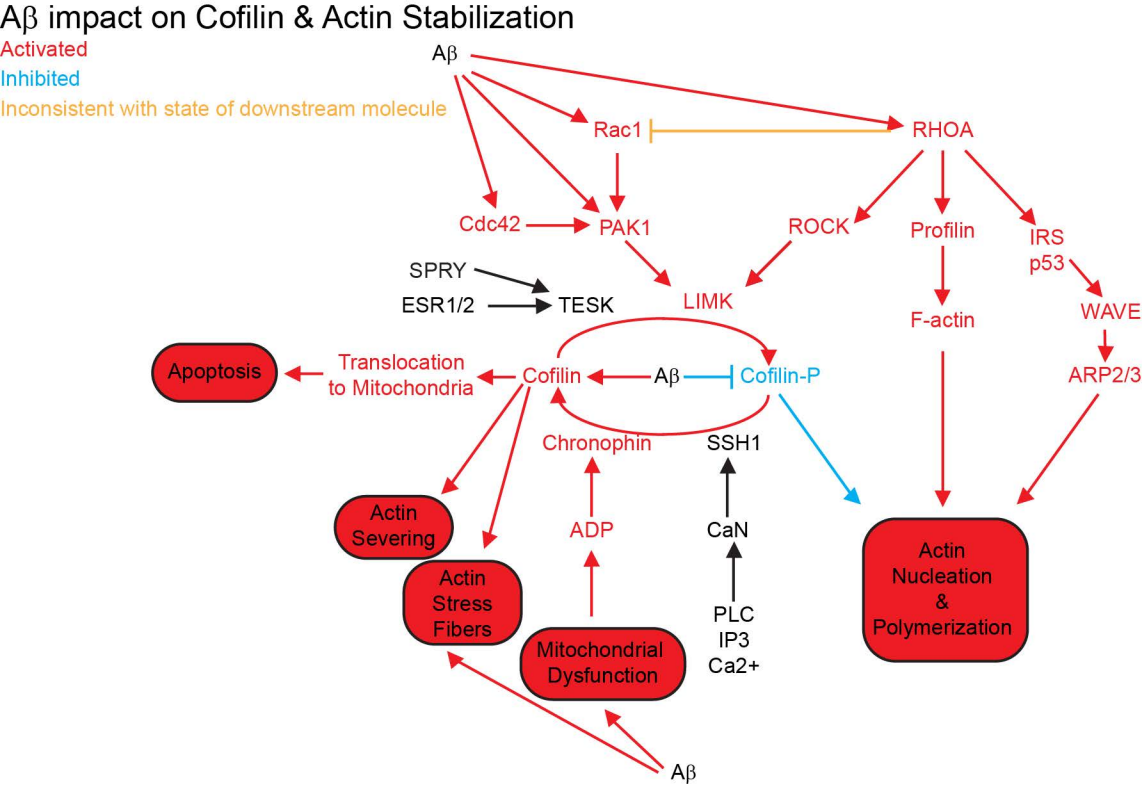
Aβ impact on Cofilin & Actin Stabilization
Activated
Inhibited
Inconsistent with state of downstream molecule
Aβ
Rac1
RHOA
Cdc42
PAK1
ROCK
Profilin
IRS
p53
SPRY
ESR1/2
TESK
LIMK
F-actin
WAVE
ARP2/3
Apoptosis
Translocation
to Mitochondria
Cofilin
Aβ
Cofilin-P
Chronophin
SSH1
Actin
Severing
ADP
CaN
Actin
Nucleation
&
Polymerization
Actin
Stress
Fibers
PLC
IP3
Ca2+
Mitochondrial
Dysfunction
Aβ